Fatigue et auto-échauffement d'alliages à mémoire de forme en NiTi avec ou sans R-phase

E. Alarcon[a,b], L. Saint-Sulpice[b], L. Heller[a], S. Arbab Chirani[b], S. Calloch[c], Petr Šittner[a]

a. Institute of Physics (Praha, République Tchèque) – 182 00 Prague, République tchèque
b. Institut de Recherche Dupuy de Lôme (IRDL FRE CNRS 3744) – École Nationale d'Ingénieurs de Brest (ENIB) – 945 Avenue Technopole, 29280 Plouzané, France
c. Institut de Recherche Dupuy de Lôme (IRDL FRE CNRS 3744) – ENSTA Bretagne – 2, rue François Verny, 29806 Brest cedex 9, France

Résumé :

Dans cette étude, les performances en fatigue structurelle de fils de NiTi est estimée en utilisant des éprouvettes en diabolo. Cette forme d'éprouvette, non-traditionnelle pour des essais de fatigue du NiTi, permet d'éviter une localisation aléatoire de la déformation au cours de l'allongement qui rend difficile l'étude de la fatigue. Des essais de fatigues pilotés e force ont étés réalisés à différentes températures et ont été complétés par des mesures d'auto-échauffement. Les résultats obtenus permettent de mettre en évidence le rôle des transformations de phase du matériau en R-phase et martensite sur la fatigue des fils de NiTi.

Abstract :

In this article the structural fatigue performance of superelastic NiTi wires is assessed using hourglass-shaped samples. This non-traditional geometry of NiTi fatigue test samples permits to avoid the random deformation localization processes upon wire deflection, which makes it difficult to interpret correctly S-N and Srain-N curves. Force controlled fatigue tests were performed at different temperatures and were complemented by self-heating measurements. The obtained results aims to shed light on the role of the phase transformations of the material into R-phase and B19' in the cyclic damaging of NiTi wires subjected to repetitive loadings.

Mots clefs : fatigue, auto-échauffement, alliage à mémoire de forme, NiTi, R-phase

Introduction

NiTi based alloys are the most widely used Shape Memory Alloys (SMA). They display an attractive combination of sound mechanical properties, biocompatibility, corrosion resistance and unique functional properties such as thermal recovery of large strains (shape memory effect), large cyclic mechanical energy absorption (vibration damping) and large reversible deformations up to 10 % (superelasticity) [2, 7]. These properties predetermine NiTi alloys for use in different engineering applications

such as medical devices[1], actuators [10, 4] and mechanical dampers [11]. In this work we focus on the superelastic capabilities of NiTi, which is achieved through a reversible stress-induced martensitic transformation. Unfortunately, wider use of cyclic superelasticity has been so far hindered by poor structural fatigue performance of NiTi that drops from millions of cycles in the linear-elastic regime down to few thousands whenever large recoverable strains are employed in engineering applications [5, 12, 3]. This issue led us to address the critical drop in fatigue performance of medical graded superelastic NiTi wires when the loading approaches the regime of the stress-induced martensitic transformation allowing for large recoverable strains (superelasticity). We address the fatigue of superelastic NiTi by employing rather original approaches consisting in the use of hourglass shaped fatigue testing samples, fatigue tests at various temperatures with regard to material characteristic phase transformation temperatures, and self-heating fatigue testing technique.

Samples geometry and material

The analysis of the fatigue behavior of superelastic NiTi wires near the onset of stress-induced martensitic transformation is hindered by localization of the transformation [12, 9, 8]. To reduce the impact of strain localization in the assessment of the fatigue performance of superelastic NiTi near the onset of martensitic transformation regime, we propose the use of hourglass shaped samples, shown in Figure 1a, instead of the traditional straight wire samples used in most of fatigue studies of NiTi wires.

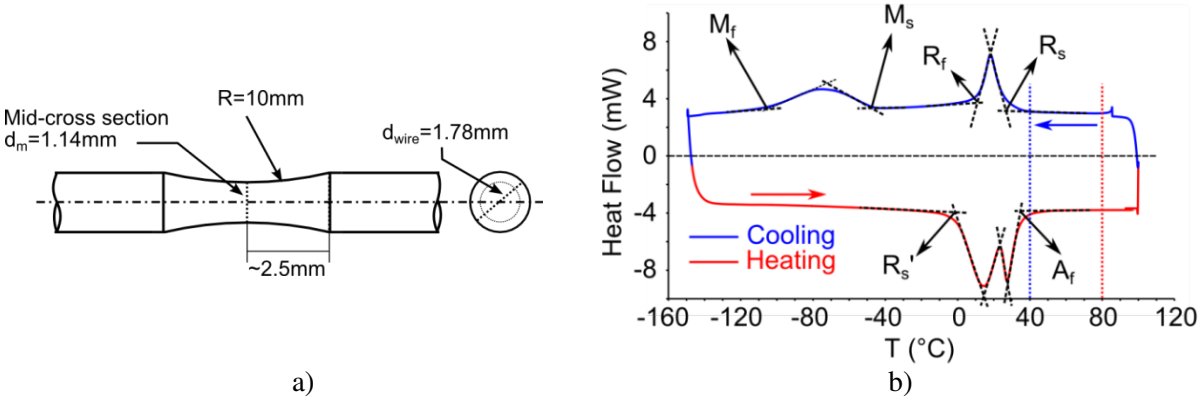

Figure 1: Geometry of hourglass shaped samples.

Compared to wire diameters usually applied in medical devices, we selected a rather large wire diameter that could be processed into the hourglass shape. We selected a cold drawn 1.78 mm NiTi wire made by Fort Wayne Metals Ltd. (FWM) from medical graded alloy denoted NiTi#1. FWM certified the final cold work of $\tilde{4}0\,\%$ and nominal composition 50.92 at. % Ni. The 5 mm long hourglass shape in the central volume of the sample is formed by grinding with a 10 mm radius grinding wheel that reduces the diameter of the sample continuously down to 1.14 mm at the mid-cross-section. After machining, the samples were electropolished in order to reduce possible surface defects. The superelastic characteristics of the samples were obtained after annealing at 500 °C during 30min followed by quenching in room temperature water. The transformation temperatures were identified using DSC as shown in Figure 1b and Table 1. It is clear for these results that three phases may interact depending on the stress and temperature conditions applied to the material: B2 asutenite, R-phase and B19' martensite.

	R_s	R_f	R'_s	A_f	M_s	M_f
T (°C)	27	11	-1	35	-48	-105

Table 1: Transformation temperatures identified from DSC measurement.

Thermomechanical response of hourglass-shaped samples

We analyzed the thermomechanical response of the concave shaped sample in order to associate the stress amplitudes and temperatures of fatigue tests with operating deformation processes. We measured the deformation and temperature fields in the concave shaped zone of hourglass-shaped samples during tensile loading by 2D Digital Image Correlation (DIC) and fast infrared thermography, respectively. To obtain the surface deformation fields associated with applied stresses by DIC, we performed quasi-static tensile tests controlled by the elongation of the arms of a clip-on extensometer of initial gauge length $L_0 = 10\,\text{mm}$ placed in the middle of the samples (Figure 2a). The nominal stress vs extensometer arms elongation curve of an hourglass shaped sample differs from the typical plateau-like response of straight wires as observed in Figure 2b. In terms of strain, below the stress threshold to induce the B19' martensitic transformation, the local response at the mid-cross section of hourglass shaped samples is the same as the strain response calculated from the elongation of the extensometer arms in straight wires $\left(\frac{\Delta L}{L_0}\right)$ (see Figure 2c). In both cases, the non-linear response is related to the austenite-to R-phase transformation that seems to develop homogeneously through the gauge length of both types of samples —within the extensometer arms in the case of straight wires and in the confined volume at the middle of hourglass shaped samples. Once the stress threshold for stress-induced B19' martensite is exceeded, large strains are localized in the middle of hourglass shaped samples as observed in the axial strain profiles 4 to 7 in Figure 2d. At this stage the local stress-strain response of hourglass shaped samples strongly differs from that of straight wires which is explained by the fact that the nucleation of the transformation in straight wires use to take place outside the gauge length covered by the extensometer —usually within the grips caused by the clamping force. This confirms that hourglass shaped samples are very effective to confine all deformation, transformation and therefore fatigue processes into a "homogeneous" representative volume at the mid-cross section. Also, this sample's shape allows for a better assessment of the stresses involved in phase transformation nucleation processes.

In order to assess the confined strain during high cycle fatigue tests performed at tens of Hz at different temperatures, where using DIC becomes more difficult, we extracted from the latest experiment a relation of the non- linear extensometer elongations with the non-linear strains associated with phase transformations at the mid-cross section of hourglass-shaped samples (Figure 2e). During tests performed without DIC, the non-linear strain obtained from the extensometer measurement is added to the elastic strains calculated by Hooke's Law to calculate the total confined strain of a tested sample. This procedure will be used when analyzing our fatigue results in the next section. In addition to DIC, we used fast thermography to associate the transformation deformation processes with nominal stresses and testing temperatures. Thermography permits to capture the heat exchange arising from forward and reverse phase transformations in superelastic NiTi. Figure 3 presents results of in-situ thermography during force-controlled tensile tests carried out at high strain rates intended to produce adiabatic conditions. The response of the materials was tested at two temperatures: 40 °C and 80 °C. For each temperature two tests were carried out; one below the stress needed to induce martensitic transformation and the second above this transformation threshold. The mechanical curves obtained for each test can be observed in Figure 3a. Mean temperature values were taken over 132 px of 15 μm pitch at the

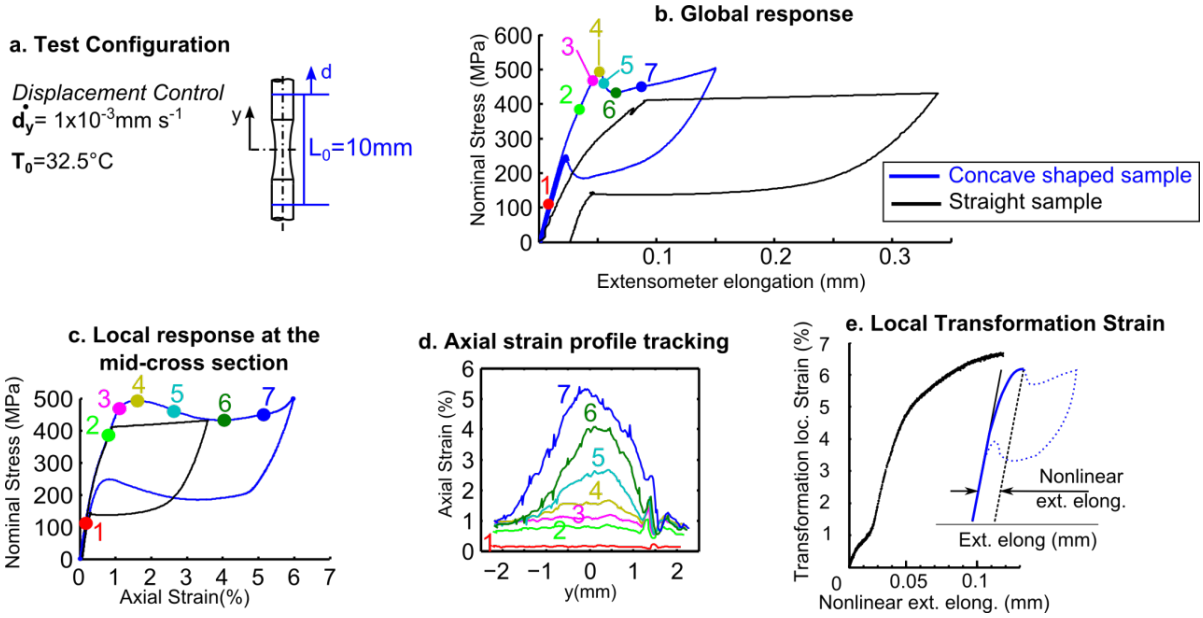

Figure 2: a) Quasi-static tensile tests configuration for DIC strain field measurements of hourglass shaped samples. b) Nominal Stress vs extensometer elongation in hourglass and straight samples. c) Nominal Stress vs local strain response extracted from the DIC strain field at the mid-cross section of hourglass-shaped samples. d) Axial unidirectional strain profiles. e) Relation between non-linear extensometer elongation and non-linear strain at the mid-cross section of hourglass-shaped samples.

mid-cross section of samples as well as 80 pixels-long axial temperature profiles. The results clearly show that the deformation through the R-phase transformation operates at a testing temperature of 40 °C when nominal stresses exceed 200 MPa as indicated by an increase in temperature due to a latent heat release associated to this phase transformation (Figure 3b). At 80 °C cooling upon loading due to thermoelastic effect prevails until the stress exceeds 590 MPa, then the temperature increases slightly before the martensitic transformation is triggered (Figure 3c). This indicates that the R-phase transformation is retarded and not fully suppressed at 80 °C. As for the B19' martensitic transformation, it appears clearly at both testing temperatures, 40 °C and 80 °C, at nominal stresses of 620 MPa and 925 MPa, respectively, as evidenced by a sharp temperature increase. These stress thresholds for B19' martensitic transformation are higher than the thresholds identified in tensile responses of quasi-static tensile tests as shown in Figure 3a. This is principally due to differences in sample's temperature caused by changes in control type and strain rates.

Fatigue results and self heating

Hourglass shaped samples were subjected to pull-pull fatigue cycling in the force-controlled regime at temperatures of 40 °C and 80 °C while the deformation was estimated from the elongation of a dynamic clip-on extensometer with 10 mm gauge length attached to the sample as explained in section 3. The applied nominal stress amplitudes involved deformations through austenite elasticity, R-phase transformation and B19' martensitic transformation. Tests were performed keeping a stress ration equal to 0.1 at a frequency of 25 Hz. Testing at 40 °C emphasized the deformation through the R-phase transformation involved in most applied amplitudes, whereas testing at 80 °C retarded the deformation through the R-phase transformation emphasizing the elastic deformation at amplitudes below the onset of the B19' martensitic transformation. Note that at 80 °C the onset of B19' martensitic transformation appears at

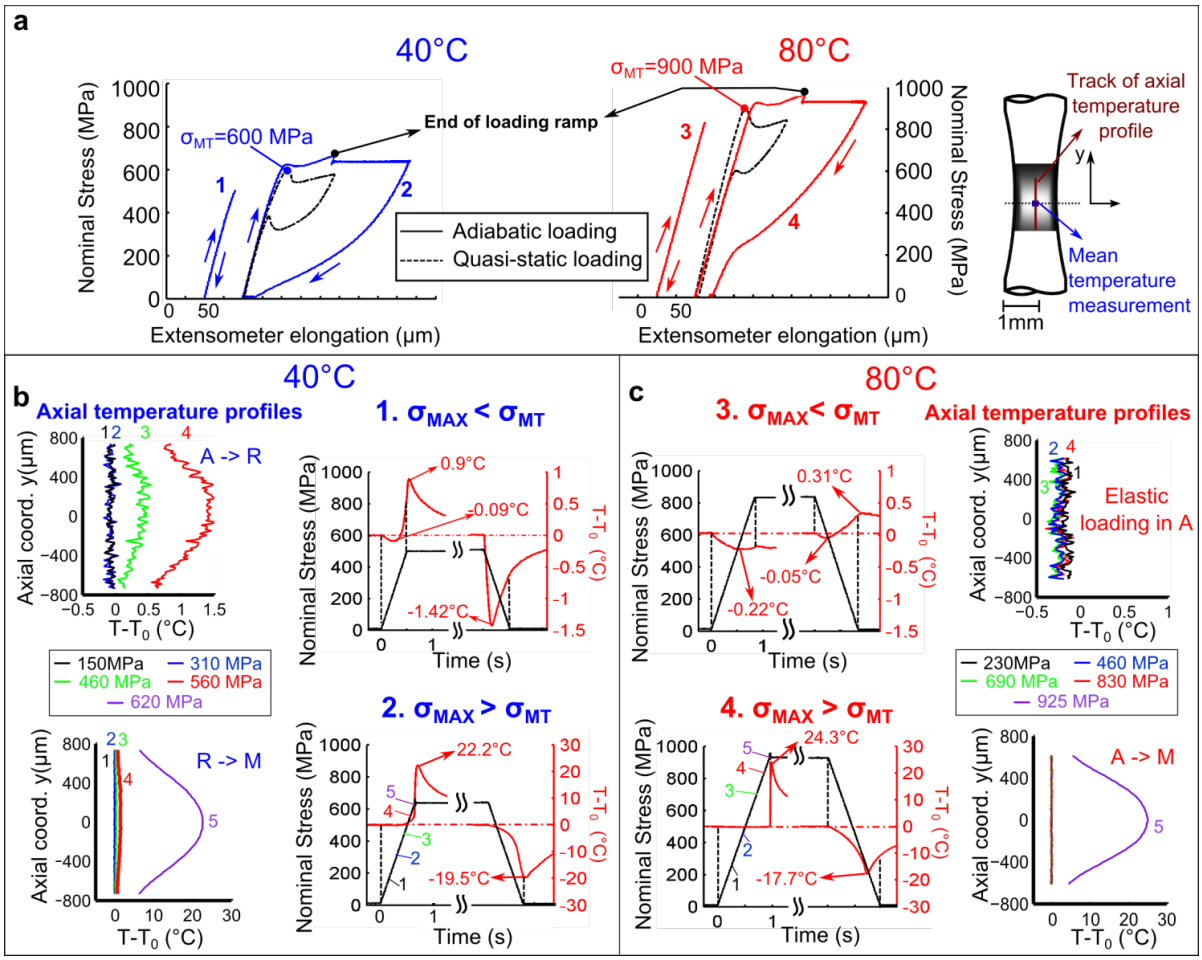

Figure 3: Thermal response during high strain rate force-controlled tensile tests. a) Tensile responses of the four tensile tests performed and comparison with quasi-static tests. b) Results from tests 1 and 2 performed at 40 °C. c) Results from tests 3 and 4 performed at 80 °C.

900 MPa while at 40 °C it appears at 600 MPa i.e. 300MPa lower (see Figure 3a). A runout of the fatigue testing was set to 1.5 million cycles. Surprisingly, the runout at 80 °C was reached at 543 MPa being 139 MPa higher compared to the value reached at 40 °C (404 MPa) as clearly seen in Figure 4a that shows the Stress-N curves identified at both the temperatures. Above the runout stresses (Sf), both the S-N curves present a continuous reduction of the number of cycles to failure. However, beside the stresses the strains play an important role in fatigue of SMAs as they do not scale linearly with stresses due to transformation deformations. Therefore, we constructed a Strain-N graph showing how the number of cycles to rupture evolves with peaks of strains in the mid-point of the samples at stabilized cycles in fatigue (Figure 4b). The marker color of each fatigue point in this figure reflects the peak of stresses applied on each test.

The Stress-N (Figure 4a). curves clearly promote elastically deforming NiTi at 80 °C as a best fatigue performer within the entire range of applied loadings. However, in the strain representation (Figure 4b)., NiTi cycled at 80 °C outperforms NiTi at 40 °C within a limited range of applied loadings with strains up to nearly 1 % (red zone in Figure 4b). Beyond this strain we approach and most probably enter the B19' martensitic transformation regime which has superior fatigue performance when induced at lower stress. We are currently working on a prediction fatigue model for NiTi wires based on the identification of the stress levels that introduce damage upon cyclic loadings. We have adopted the self-heating methodology,

a)

b)

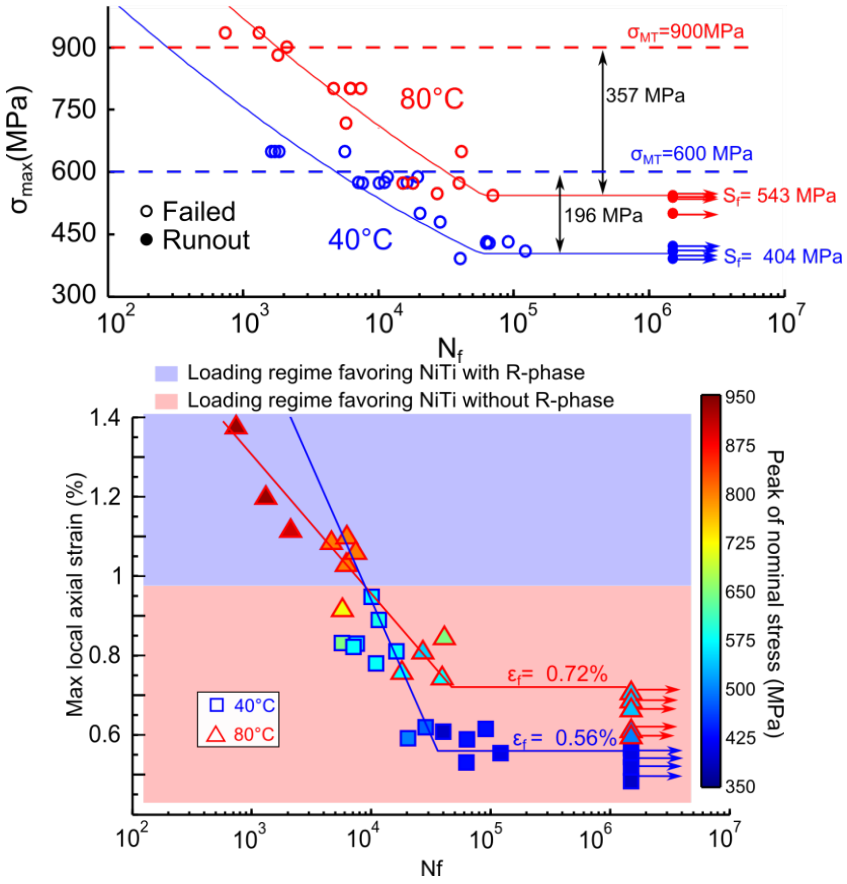

Figure 4: Fatigue results at 40 °Cand 80 °C. a) Stress-N curves. b) Strain-N curves illustrating the stress by the inner-color of the markers.

successfully employed for predicting the high cycle fatigue life of other alloys [6]. As the first step, we have tracked the mean temperature elevation during cyclic tests carried out at 25 Hz, stress ratio 0.1 at 25 °C, 40 °C and 80 °C for different maximum stress values. These results can be observed in Figure 4. Due to R-phase transformation, lower temperature testing induces earlier and higher mean temperature elevation associated to the amount of energy dissipated per cycle. This goes in agreement with fatigue results in Figure 4 that shows worse high cycle fatigue performance when R-phase transformation regime was entered. Ongoing complementary experiments are being carried out to determine the sources of this dissipated heat.

Conclusions and perspectives

The structural fatigue of superelastic NiTi wires has been tested at two temperatures in order to assess the effect of phase transformations on their performance in the High Cycle Fatigue regime. Hourglass-shaped samples have been used in order to prevent random localization of the transformation / deformation / stress observed in traditional straight samples used in fatigue tests of NiTi wires. The intermediate phase transformation known as R-phase seems to worsen the fatigue properties of the materials as it has been shown in S-N, Strain-N and self-heating curves. The ongoing work attempts to propose a life prediction modeling solution to take into account this effect.

References

[1] T. Duerig, A. Pelton, and D. Stöckel. An overview of nitinol medical applications. *Materials Science and Engineering: A*, 273–275:149–160, December 1999.

[2] T. W. Duerig, K. N. Melton, D. Stöckel, and C. M. Wayman. *Engineering Aspects of Shape Memory Alloys*. Butterworth-Heinemann, 1990. DOI: 10.1016/B978-0-7506-1009-4.50001-9.

[3] A. M. Figueiredo, P. Modenesi, and V. Buono. Low-cycle fatigue life of superelastic NiTi wires. *International Journal of Fatigue*, 31(4):751–758, April 2009.

[4] Y. Fu, H. Du, W. Huang, S. Zhang, and M. Hu. TiNi-based thin films in MEMS applications: a review. *Sensors and Actuators A: Physical*, 112(2–3):395–408, May 2004.

[5] M. B. McGuigan, C. Louca, and H. F. Duncan. Endodontic instrument fracture: causes and prevention. *British Dental Journal*, 214(7):341–348, April 2013.

[6] R. Munier, C. Doudard, S. Calloch, and B. Weber. Determination of high cycle fatigue properties of a wide range of steel sheet grades from self-heating measurements. *International Journal of Fatigue*, 63:46–61, June 2014.

[7] K. Otsuka and X. Ren. Physical metallurgy of Ti–Ni-based shape memory alloys. *Progress in Materials Science*, 50(5):511–678, July 2005.

[8] P. Sedmák, P. Šittner, J. Pilch, and C. Curfs. Instability of cyclic superelastic deformation of NiTi investigated by synchrotron X-ray diffraction. *Acta Materialia*, 94:257–270, August 2015.

[9] P. Sittner, Y. Liu, and V. Novak. On the origin of Lüders-like deformation of NiTi shape memory alloys. *Journal of the Mechanics and Physics of Solids*, 53(8):1719–1746, August 2005.

[10] D. Stoeckel. Shape memory actuators for automotive applications. *Materials & Design*, 11(6):302–307, December 1990.

[11] C. Van der Eijk, J. S. Olsen, and Z. Zhang. Application of NiTi Shape Memory Alloy Dampers in Civil Structures. In *Proceedings of the First International Conference on Self Healing Materials*, Noordwijk aan Zee, The Netherlands, April 2007.

[12] L. Zheng, Y. He, and Z. Moumni. Lüders-like band front motion and fatigue life of pseudoelastic polycrystalline NiTi shape memory alloy. *Scripta Materialia*, 123:46–50, October 2016.